# Offset-free Model Predictive Control for a Cone-shaped Active Magnetic Bearing System

Luis M. Castellanos*, Angelo Bonfitto, Renato Galluzzi

*Department of Mechanical and Aerospace Engineering (Mechatronics Laboratory), Politecnico di Torino, Corso Duca degli Abruzzi, 24, Turin, Italy.*

**Abstract**

Active Magnetic Bearings (AMB) are mechatronic systems that support a rotating shaft using magnetic levitation. The standard AMB architecture includes two radial and one axial actuator. An alternative geometry with cone-shaped magnetic cores allows for a more compact layout without a dedicated axial actuator. However, this configuration reduces the axial force generation capability and requires a more complex control architecture due to the inherent coupling of the axial and radial control actions. When using decentralized control, effective handling of the coil current limitations together with the axial disturbance rejection is difficult to achieve. In this context, the present paper demonstrates the benefits of applying Offset-Free Model Predictive Control (OF-MPC) for a cone-shaped AMB system. A procedure for the overall design is presented and supported by the experimental work conducted in a scaled machine that reproduces an on-board turbo-compressor unit for an aircraft. The modeling of the system is described together with the design of the OF-MPC in all its parts: general control architecture, disturbance model and observer design, target calculation and control problem formulation. An OF-MPC variant with reduced control horizon is proposed and implemented in real time. Experimental results demonstrate that the prototype is compliant with application-specific stability requirements from the ISO 14839-3:2006 standard. In addition, experiments show that OF-MPC outperforms decentralized PID controllers in terms of axial disturbance rejection. OF-MPC yields a favorable constrained optimal control technique for cone-shaped AMBs because intrinsic coupling and current saturation are optimally handled by the controller.

*Keywords:* Active magnetic bearings, cone-shaped, model predictive control, offset-free, magnetic levitation

## 1. Introduction

Active Magnetic Bearings (AMBs) are commonly adopted in several industrial fields, such as vacuum, oil and gas, manufacturing, medical and refrigeration applications to attain contactless operation of rotating machines [1]. They are used to support the rotor of turbo-compressors, turbo-blowers, vacuum pumps and high-speed mandrels and feature a series of remarkable advantages, like the absence of friction and lubricants, reduction of power losses, non-contaminated environment, possibility of reaching higher rotational speeds, online adjustment of the operating conditions, and remote continuous monitoring [2]. Recently, the research on AMBs has been mainly focused on the study of new actuator geometries and materials [3, 4, 5], development of advanced sensing and sensorless strategies [6, 7, 8], definition of more effective control strategies [9, 10, 11], integration of the levitation and motor tasks in the so-called bearingless configurations [12, 13, 14], and reduction of cost, weight and size [15, 16].

Typically, an active magnetic suspension exploits three actuation stages, two for the radial degree of freedom (DOF) and one for the axial control. This standard architecture needs a dedicated thrust bearing, which is bulky and hinders the maximum spin speed because of magnetic losses and centrifugal stress on the actuator disc. Moreover, the presence of the thrust bearing lengthens the shaft, with negative consequences for the rotordynamic behavior. Therefore, the elimination of the thrust bearing could lead to a more integrated layout that exploits only two planes of actuation for the generation of both radial and axial levitation forces. This solution can be implemented by using a conical geometry for the pole pieces and finds its application where compactness is an important requirement [17, 18, 19]. Although promising, the adoption of cone-shaped AMBs in industrial applications has been strongly limited by a series of drawbacks, such as the low axial force generation capability and the challenging synthesis of the control strategy due to the coupling of the axial and radial control actions [20]. The current on each electromagnet is indeed the sum of axial and radial control contributions. Therefore, each controller oversees its own contribution, while neglecting the total current flowing through the coils. In the case of relevant axial perturbation, coil current saturation may occur and cause negative effects on the stability. This problem is partially addressed in the literature by handling current limitations externally and not within the controller. To the authors' knowledge, the literature dedicated to conical AMB systems is scarce. A previous work presents decoupled Proportional-Integral-Derivative (PID) controllers for a cone-shaped AMB system [21]. Numerical analyses with a

*Corresponding author
*Email addresses:* luis.castellanos@polito.it (Luis M. Castellanos), angelo.bonfitto@polito.it (Angelo Bonfitto), renato.galluzzi@polito.it (Renato Galluzzi)

centralized fuzzy controller are presented in [22, 23].

In modern control theory, Model Predictive Control (MPC) is a promising technique that has been gaining increasing attention recently. As a centralized strategy, MPC is able to optimally handle the trade-off between control effort and controlled outputs by taking into account plant dynamics and constraints [24]. Although the study of MPC for active magnetic levitation is not new, it has never been applied to conical AMBs. The benefits of using linear and nonlinear MPC in the case of single-DOF active magnetic levitation have been demonstrated numerically and experimentally [25, 26]. A numerical comparison between MPC and conventional PID controllers is presented in [27, 28] for flywheel energy storage systems. Despite these efforts, the state of the art fails at addressing properly the experimental validation of MPC for magnetically suspended rotors. One of the possible motivations is the inherent computational burden of this approach: in the online version, an optimization problem is solved at each fundamental time step, whereas in the offline explicit variant, the state assessment is required at each iteration.

The present paper proposes the implementation of MPC in cone-shaped AMB systems. This technique offers promising features to optimally handle the coil current saturation. The method presented here is a variant of MPC known as Offset-Free Model Predictive Control (OF-MPC) [29, 30, 31]. The term "Offset-Free" refers to the possibility of guaranteeing zero-offset at steady state, based on the external disturbance estimate. The application of OF-MPC is suitable for conical-shaped AMB systems because it allows handling effectively the coupling of radial and axial control actions, and the effects of the low axial force generation capability.

In this work, the application of OF-MPC is conducted on a reduced-scale turbo-compressor prototype for refrigeration tasks inside an aircraft. The rotor of this machine is suspended by conical AMBs. The system modeling and OF-MPC design are described with a particular focus on control problem formulation, augmented model with external disturbances as additional states, observer design for the augmented model, and target calculation. The observer is based on a Kalman filter designed to handle effectively the trade-off between noise rejection and margin recovery. An online OF-MPC formulation with reduced control horizon is proposed to reduce the computational overhead allowing the real-time implementation.

Experiments were conducted as follows. At first, the controlled plant behavior was evaluated in a lifting-up test that takes the rotor from rest to the nominal position. Then, the closed-loop performance was assessed by verifying that the peaks of the output sensitivity functions comply with the AMB-specific ISO 14839-3:2006 standard [32]. Finally, transient-response analyses are conducted with three different settings of OF-MPC to validate the control design approach. To provide means for a fair benchmark, the OF-MPC was compared to conventional PIDs synthesized from the OF-MPC problem formulation. This approach enables a proper confrontation among techniques, where the obtained controllers behave as similarly as possible around the nominal position.

The main contributions of this work are: a) the proposal of a control method to handle effectively coil current saturation, axial-radial coupling and low axial force generation capability in cone-shaped AMBs; b) the experimental validation of an online MPC technique with a reduced control horizon on a conical AMB system; c) the definition of an MPC design procedure to guarantee an output disturbance rejection compliant with the requirement of the ISO 14839-3:2006 standard.

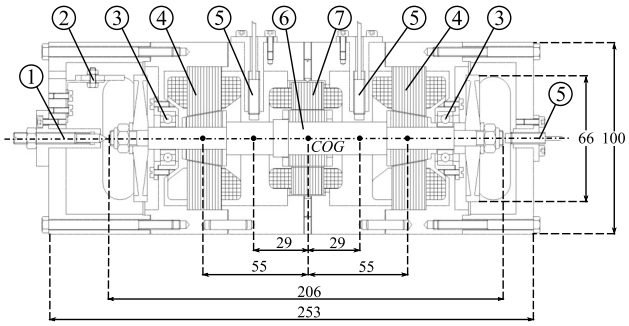


Figure 1: Section view of the machine. 1) Centering tip. 2) Spin speed sensor. 3) Landing bearings. 4) Magnetic actuators. 5) Inductive displacement sensors. 6) Rotor. 7) Electric motor. Dimensions are in mm.

The work is organized as follows. The plant under study is described and modeled in Sec. 2. The actuator configuration is described in Sec. 3. Section 4 outlines the control strategy in detail. Experimental results are presented in Sec. 5. Finally, Sec. 6 concludes the work.

## 2. Plant model

The plant under study is a downscaled reproduction of a turbo-compressor group of a conditioning unit used in a jet aircraft. Figure 1 illustrates the longitudinal section view of the machine. The conical geometry of the magnetic bearings allows performing a compact design of the actuation stage which is composed of only four pairs of electromagnets instead of five of the conventional cylindrical solution, thus awakening great interest for the application in compact machines.

Turbine and compressor impellers are simulated by two mock-up discs of steel. The first two flexible rotor modes were numerically evaluated at 10831 rad/s and 31331 rad/s, respectively. Corresponding critical speeds are beyond the maximum rotational speed of the machine (24 krpm).

Figure 2 shows the electromagnetic forces $(F_1, ..., F_8)$ produced by the eight electromagnets placed on the stator. These forces are generated by varying the coil currents to control the shaft position. Tables 1 and 2 list the main parameters of the system.

Assuming that the rotor is rigid, and considering the gyro-

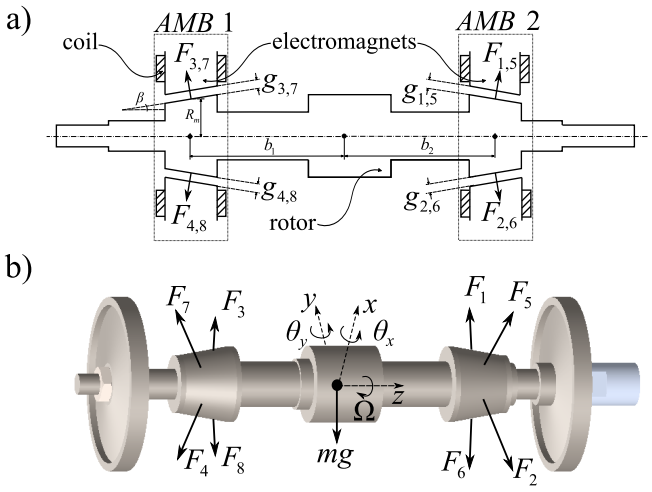


Figure 2: a) Forces on Y-Z and X-Z planes. b) 3D projection of the motor shaft with the corresponding electromagnetic forces, and with the two discs that simulate the turbine and compressor impellers inserted.

Table 1: Rotor parameters

| Symbol | Name | Value | Unit |
|---|---|---|---|
| $g_0$ | Nominal air gap | 0.45 | mm |
| $m$ | Rotor mass | 0.755 | kg |
| $J_p$ | Polar moment of inertia | $1.54 \cdot 10^{-4}$ | kgm$^2$ |
| $J_d$ | Diametral moment of inertia | $31.68 \cdot 10^{-4}$ | kgm$^2$ |
| $\beta$ | Magnetic core inclined angle | 0.98 | rad |
| $b_1$ | Distance between bearing (1) and COG | 55 | mm |
| $b_2$ | Distance between bearing (2) and COG | 55 | mm |
| $c_1$ | Distance between bearing (1) sensor and COG | 29 | mm |
| $c_2$ | Distance between bearing (2) sensor and COG | 29 | mm |
| $R_m$ | Effective radius | 12.4 | mm |

scopic effects [33], the equations of motion can be written as

$$\begin{aligned} m\ddot{z} = {} & (F_1 + F_2 + F_5 + F_6)\sin\beta \\ & - (F_3 + F_4 + F_7 + F_8)\sin\beta + F_z \end{aligned} \tag{1}$$

$$m\ddot{x} = (F_5 - F_6 + F_7 - F_8)\cos\beta + F_x \tag{2}$$

$$m\ddot{y} = (F_1 - F_2 + F_3 - F_4)\cos\beta + F_y \tag{3}$$

$$\begin{aligned} J_d\ddot{\theta}_x = {} & [(F_1 - F_2)\,b2 + (F_4 - F_3)\,b_1]\cos\beta \\ & + (F_2 - F_1 + F_3 - F_4)\,R_m\sin\beta - J_p\Omega\dot{\theta}_y + M_x \end{aligned} \tag{4}$$

$$\begin{aligned} J_d\ddot{\theta}_y = {} & [(F_6 - F_5)\,b2 + (F_7 - F_8)\,b_1]\cos\beta \\ & + (F_5 - F_6 + F_8 - F_7)\,R_m\sin\beta + J_p\Omega\dot{\theta}_x + M_y \end{aligned} \tag{5}$$

where $F_z$, $F_x$, $F_y$ are generalized disturbance forces acting on $x$, $y$, and $z$ directions, respectively, and $M_x$, $M_y$ are moments around x-axis and y-axis, respectively; $\Omega$ stands for the spin speed; and the electromagnetic forces are given by

$$F_j = K\frac{i_j^2}{g_j^2};\ j = 1, ..., 8, \tag{6}$$

Table 2: Actuator parameters

| Symbol | Name | Value | Unit |
|---|---|---|---|
| $N$ | Coil turns | 82 | – |
| $R$ | Coil resistance | 0.5 | $\Omega$ |
| $L_0$ | Nominal inductance | 1.2 | mH |
| $S$ | Pole cross-sectional area | 118 | mm$^2$ |

with the force coefficient

$$K = \frac{\mu_0 S N^2 \cos\sigma}{4} \tag{7}$$

in which $\sigma = \pi/8$ is the angle of each pole relative to the centerline between the poles, and $\mu_0 = 4\pi\cdot 10^{-7}$ H/m is the vacuum magnetic permeability.

The bearing air gaps $g_j$ presented in Eq. 6 can be referred to the center of gravity (COG) coordinates involving the geometrical quantities introduced in Fig. 2 as

$$g_{1,2} = g_0 - z\sin\beta \mp \cos\beta(y + b_2\theta_x) \tag{8}$$

$$g_{3,4} = g_0 + z\sin\beta \mp \cos\beta(y - b_1\theta_x) \tag{9}$$

$$g_{5,6} = g_0 - z\sin\beta \mp \cos\beta(x - b_2\theta_y) \tag{10}$$

$$g_{7,8} = g_0 + z\sin\beta \mp \cos\beta(x + b_1\theta_y). \tag{11}$$

Let $\boldsymbol{\zeta}$ denote the state vector $[z, x, y, \theta_x, \theta_y, \dot{z}, \dot{x}, \dot{y}, \dot{\theta}_x, \dot{\theta}_y]^\intercal$, $\boldsymbol{i}$ the vector of coils currents $[i_1, ..., i_8]^\intercal$ and $\boldsymbol{d}$ the vector of disturbances $[F_z,\ F_x,\ F_y,\ M_x,\ M_y]^\intercal$. The state equations can be compactly written by substituting the air gap expressions (Eqs. 8 to 11) into Eq. 6 and then into the motion formulation (Eqs. 1 to 5):

$$\dot{\boldsymbol{\zeta}} = \boldsymbol{h}(\boldsymbol{\zeta}, \boldsymbol{i}, \boldsymbol{d}, \Omega), \tag{12}$$

thus yielding a condensed nonlinear time-domain representation of the system.

## 3. Magnetic bearings actuation

In conventional AMB systems, the actuation along one axis of control is obtained as the sum of the contributions of two opposite electromagnets. They are typically operated in differential driving mode, i.e. one electromagnet is driven with the sum of a bias and a control current ($i_0 + i_{cj}$), while the opposite one with their difference ($i_0 - i_{cj}$) [1]. The same principle is applied also for conical AMBs in the axial direction. By inspecting Fig. 2, any positive deviation along $z$ from the equilibrium point can be compensated by increasing forces $F_{3,4,7,8}$ (AMB 1) and decreasing forces $F_{1,2,5,6}$ (AMB 2) simultaneously. The opposite condition can be verified in the case of negative deviations. Figure 3 depicts this control strategy with the differential driving mode configuration.

Five control currents $\boldsymbol{u} = [u_z, u_{x_1}, u_{y_1}, u_{x_2}, u_{y_2}]^\intercal$ are used to control the five-DOF plant. The coil currents can be expressed

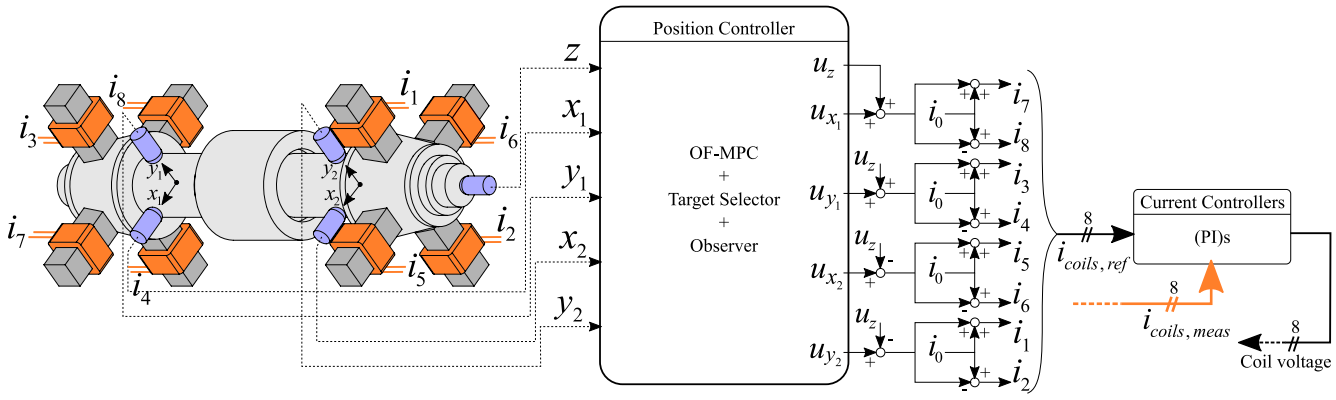


Figure 3: Control diagram with the transformation from control to coil currents. Subscripts *ref* and *meas* stand for *references* and *measurements*, respectively.

in terms of control actions along the motion directions as

$$\begin{bmatrix} i_1 \\ i_2 \\ i_3 \\ i_4 \\ i_5 \\ i_6 \\ i_7 \\ i_8 \end{bmatrix} = i_0 + \underbrace{\begin{bmatrix} 1 & 0 & 0 & 0 & 1 \\ 1 & 0 & 0 & 0 & -1 \\ -1 & 0 & 1 & 0 & 0 \\ -1 & 0 & -1 & 0 & 0 \\ 1 & 0 & 0 & 1 & 0 \\ 1 & 0 & 0 & -1 & 0 \\ -1 & 1 & 0 & 0 & 0 \\ -1 & -1 & 0 & 0 & 0 \end{bmatrix}}_{K_u} \begin{bmatrix} u_z \\ u_{x_1} \\ u_{y_1} \\ u_{x_2} \\ u_{y_2} \end{bmatrix}, \qquad (13)$$

in which $K_u \in \mathbb{R}^{n_{coils} \times n_u}$, with $n_{coils} = 8$, is the transformation matrix between control actions and coil current deviations.

### 3.0.1. Actuator dynamics

Proportional-Integral (PI) current controllers are designed to speed up the actuator response. All the electromagnets are considered identical and the selected PI integral time $\tau_i$ cancels the open-loop time constant of the coils (i.e. $\tau_i = L_0/R$). The resulting coil current dynamics can be modeled by the differential equations

$$\dot{i}_j = -\omega_{cl} i_j + \omega_{cl} i_{j,ref}, \; j = 1, ..., 8, \qquad (14)$$

where $i_{j,ref}$ is current reference for coil $j$ and $\omega_{cl}$ is the bandwidth of the current loop. The latter can be theoretically defined as $\omega_{cl} = K_p/L_0$ where $K_p = 40$ V/A is the proportional gain. However, from preliminary experimental tests, the bandwidth resulted about 1 kHz due to voltage saturation. Nevertheless, these dynamics are considered much faster than the mechanical ones and hence neglected when modeling the mechanical plant. Therefore, while dealing with mechanical dynamics, it is assumed that the coil current references obtained from Eq. 13 are the actual currents flowing through the coils.

## 4. Linear OF-MPC formulation

The model in Eq. 12 may deviate from the real plant due to unmodeled dynamics, unknown disturbances, uncertain system parameters or modeling errors. Furthermore, the plant under study belongs to an aircraft, with disturbance forces that can change over time due to flight maneuvering. The possibility to optimally handle the plant-model mismatch is offered by the Offset-Free Model Predictive Control (OF-MPC). It guarantees zero-offset tracking by adding an integral action from the knowledge of the plant-model mismatch, while the controller design is an automated design procedure based on the trade-off between the control effort and the error in the controlled variables. Figure 4 shows the OF-MPC control scheme. The observer estimates both state and disturbances which are used by the target calculator together with the reference vector $\boldsymbol{r}$ to obtain the input and state targets. Both target vectors together with the state and disturbance estimates are used to initialize the OF-MPC control problem.

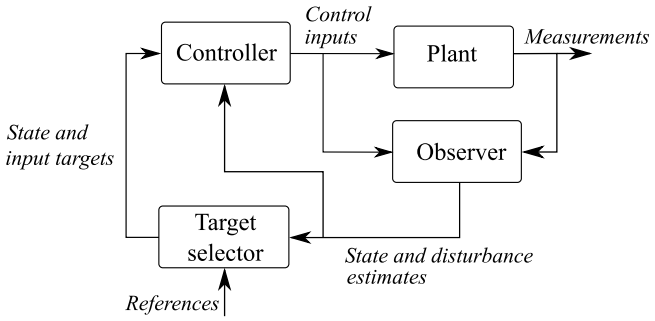


Figure 4: OF-MPC control scheme consisting of: controller, state estimator, and target selector.

### 4.1. Linear model

The nonlinear plant model in Eq. 12 is linearized at nominal air gap $g_0$ with all the coil currents equal to the bias current $i_0 = 1.5$ A and at standstill ($\Omega = 0$). This linear model will be later adopted in the linear OF-MPC formulation. Linearization is performed using Taylor series expansion

$$\dot{\boldsymbol{\zeta}} \doteq \underbrace{\left.\frac{\partial h}{\partial \boldsymbol{\zeta}}\right|_0}_{\bar{A}} (\boldsymbol{\zeta} - \boldsymbol{\zeta_0}) + \underbrace{\left.\frac{\partial h}{\partial \boldsymbol{i}}\right|_0}_{\bar{B}_i} (\boldsymbol{i} - \boldsymbol{i_0}) + \underbrace{\left.\frac{\partial h}{\partial \boldsymbol{d}}\right|_0}_{\bar{B}_d} (\boldsymbol{d} - \boldsymbol{d_0}). \qquad (15)$$

Denoting the coil current $i_j = i_{cj} + i_0$, $j = 1, ..., 8$ and knowing that $\boldsymbol{\zeta} = \boldsymbol{\zeta} - \boldsymbol{\zeta_0}$ since $\boldsymbol{\zeta_0} = \boldsymbol{0}$, Eq. 15 results in

$$\dot{\boldsymbol{\zeta}} = \bar{A}\boldsymbol{\zeta} + \bar{B}_i \boldsymbol{i_c} + \bar{B}_d \boldsymbol{d}, \qquad (16)$$

where $\boldsymbol{i_c}$ is the vector of coil current deviations.

The coil current deviation vector can be expressed in terms of the control current vector $\boldsymbol{u}$:

$$\boldsymbol{i_c} = K_u \boldsymbol{u}, \tag{17}$$

and hence, Eq. 16 becomes

$$\dot{\boldsymbol{\zeta}} = \bar{A}\boldsymbol{\zeta} + \underbrace{\bar{B}_i K_u}_{\bar{B}} \boldsymbol{u} + \bar{B}_d \boldsymbol{d} \tag{18}$$

with

$$\bar{A}_{10\times10} \begin{cases} a_{1,6} = a_{2,7} = a_{3,8} = a_{4,9} = a_{5,10} = 1 \\ a_{6,1} = 3634 \\ a_{7,2} = a_{8,3} = 58434 \\ a_{9,4} = a_{10,5} = 39838 \\ a_{i,j} = 0 \text{ elsewhere} \end{cases} \tag{19}$$

$$\bar{B}_{10\times5} \begin{cases} b_{6,1} = 6.28 \\ b_{7,2} = a_{7,4} = a_{8,3} = a_{8,5} = 8.9 \\ b_{9,3} = a_{10,4} = -111.2 \\ b_{9,5} = a_{10,2} = 111.2 \\ b_{i,j} = 0 \text{ elsewhere} \end{cases} \tag{20}$$

$$\bar{B}_{d,10\times5} \begin{cases} b_{d,6,1} = b_{d,7,2} = b_{d,8,3} = 1.32 \\ b_{d,9,4} = a_{d,10,5} = 315.66 \\ b_{d,i,j} = 0 \text{ elsewhere.} \end{cases} \tag{21}$$

Due to the mathematical complexity of the linearization process, the Jacobian matrices are parametrically obtained and evaluated using MATLAB's Symbolic Math Toolbox.

#### 4.1.1. Sensor coordinates

Equation 18 is the plant model referenced to the COG coordinates $(z, x, y, \theta_x, \theta_y)$. However, in this work, a transformation into the sensor coordinates $(z, x_1, y_1, x_2, y_2)$ is preferred. The displacement sensors installed on the plant fix the sensor coordinates comprised in

$$\begin{bmatrix} z \\ x_1 \\ y_1 \\ x_2 \\ y_2 \end{bmatrix} = \underbrace{\begin{bmatrix} 1 & 0 & 0 & 0 & 0 \\ 0 & 1 & 0 & 0 & c_1 \\ 0 & 0 & 1 & -c_1 & 0 \\ 0 & 1 & 0 & 0 & -c_2 \\ 0 & 0 & 1 & c_2 & 0 \end{bmatrix}}_{T} \begin{bmatrix} z \\ x \\ y \\ \theta_x \\ \theta_y \end{bmatrix}. \tag{22}$$

Let $\boldsymbol{q} = [z,\ x_1,\ y_1,\ x_2,\ y_2,\ \dot{z},\ \dot{x}_1,\ \dot{y}_1,\ \dot{x}_2,\ \dot{y}_2,\ \dot{z}]^\intercal$ denote the plant state referenced to the sensor coordinates, hence

$$\boldsymbol{q} = \mathcal{T}\boldsymbol{\zeta}, \tag{23}$$

in which $\mathcal{T} = blockdiag(T, T)$ is the state transformation matrix from the COG coordinates. Substituting $\boldsymbol{\zeta}$ from Eq. 23 into 18 results in

$$\dot{\boldsymbol{q}} = \underbrace{\mathcal{T}\bar{A}\mathcal{T}^{-1}}_{\tilde{A}} \boldsymbol{q} + \underbrace{\mathcal{T}\bar{B}}_{\tilde{B}} \boldsymbol{u} + \underbrace{\mathcal{T}\bar{B}_d\mathcal{T}^{-1}}_{\tilde{B}_d} \boldsymbol{d}. \tag{24}$$

Applying exact discretization to Eq. 24 with sampling time $T_s = 0.25$ ms yields

$$\begin{aligned} \boldsymbol{q}(k+1) &= A\boldsymbol{q}(k) + B\boldsymbol{u}(k) + B_d\boldsymbol{d}(k), \\ \boldsymbol{y} &= C\boldsymbol{q}(k). \end{aligned} \tag{25}$$

With $C = [I_{5\times5}\ \mathbf{0}_{5\times5}]$ on the output equation, the previous set can be converted into a discrete-time linear state-space representation of the plant under study. It will be used as the internal model of the OF-MPC controller.

### 4.2. Linear augmented model

To guarantee offset-free control of the output $\boldsymbol{y}$ in the presence of plant/model mismatch and/or unmeasured disturbances, the plant model (Eq. 25) is augmented with an integrating disturbance according to the general methodology proposed by Pannocchia and Rawlings [34]. This methodology requires adding a number of integrating disturbances equal to the number of measured variables in a way that the resulting augmented system is detectable. To this aim, infinite choices are available. In this work, the so-called *input disturbance model* is used. It consists of adding an integrating state $\boldsymbol{d}$ that enters the system at the same place as the inputs $\boldsymbol{u}$. Several studies have pointed out that such a model is an appropriate choice for efficiently rejecting unmeasured disturbances [35, 36, 37]. By inspecting Eq. 25, it can be seen that external disturbances are already modeled as unmeasured external forces $\boldsymbol{d}$. The resulting augmented system is presented in discrete-time domain as follows

$$\begin{aligned} \begin{bmatrix} \boldsymbol{q}(k+1) \\ \boldsymbol{d}(k+1) \end{bmatrix} &= \underbrace{\begin{bmatrix} A & B_d \\ 0_{n_d\times n_q} & I_{n_d\times n_d} \end{bmatrix}}_{A_{aug}} \begin{bmatrix} \boldsymbol{q}(k) \\ \boldsymbol{d}(k) \end{bmatrix} \\ &\quad + \underbrace{\begin{bmatrix} B \\ \mathbf{0}_{n_d\times n_u} \end{bmatrix}}_{B_{aug}} \boldsymbol{u} + \begin{bmatrix} \boldsymbol{w}_q(k) \\ \boldsymbol{w}_d(k) \end{bmatrix} \end{aligned} \tag{26}$$

$$\boldsymbol{y}_m(k) = [C\ \mathbf{0}_{n_y\times n_d}] \begin{bmatrix} \boldsymbol{q}(k) \\ \boldsymbol{d}(k) \end{bmatrix} + \boldsymbol{w}_n(k). \tag{27}$$

where $\boldsymbol{w}_q \in \mathbb{R}^{n_q}$ and $\boldsymbol{w}_d \in \mathbb{R}^{n_d}$ represent the state and disturbance noise, respectively; $\boldsymbol{y}_m$ stands for the measurements, i.e., the model output $\boldsymbol{y}$ corrupted by the measurement noise $\boldsymbol{w}_n \in \mathbb{R}^{n_y}$. With some abuse of notation, the added disturbances are named $\boldsymbol{d}(k)$. It means that hereinafter, the estimates $\hat{\boldsymbol{d}}$ will lump not only the real external forces but also the plant-model mismatch. The number of states, disturbances and measurements are denoted by $n_q = 10$, $n_d = 5$, and $n_y = 5$, respectively.

### 4.3. Disturbance estimator and target calculation

If the augmented plant model is detectable, the following estimator can be implemented to get the state $\hat{\boldsymbol{q}}(k)$ and the disturbance $\hat{\boldsymbol{d}}(k)$ estimates based on the measurements $\boldsymbol{y_m}$ and in-

puts $\boldsymbol{u}$:

$$\begin{aligned}\begin{bmatrix} \hat{\boldsymbol{q}}(k+1) \\ \hat{\boldsymbol{d}}(k+1) \end{bmatrix} &= \begin{bmatrix} A & B_d \\ 0_{n_d \times n_q} & I_{n_d \times n_d} \end{bmatrix} \begin{bmatrix} \hat{\boldsymbol{q}}(k) \\ \hat{\boldsymbol{d}}(k) \end{bmatrix} \\ &+ \begin{bmatrix} B \\ 0_{n_d \times n_u} \end{bmatrix} \boldsymbol{u}(k) \\ &+ \begin{bmatrix} L_q \\ L_d \end{bmatrix} (\boldsymbol{y_m}(k) - C\hat{\boldsymbol{q}}(k)) \end{aligned} \tag{28}$$

where $L_q \in \mathbb{R}^{n_q}$ and $L_d \in \mathbb{R}^{n_d}$ are the predictor gain matrices for the state and the disturbance, respectively. They are obtained using the Kalman filter design approach, based on the information of the noise intensities. The process noise inputs $[\boldsymbol{w_q}\ \boldsymbol{w_d}]$ and measurement noise inputs $\boldsymbol{w_n}$ belong to uncorrelated zero-mean Gaussian stochastic processes with covariance matrices $W_0$ and $V_0$ given by

$$\begin{aligned} W_0 &= blockdiag(var\{\boldsymbol{w_q}\}, var\{\boldsymbol{w_d}\}), \\ V_0 &= var\{\boldsymbol{w_n}\}. \end{aligned} \tag{29}$$

The variances $var\{\cdot\}$ of $\boldsymbol{w_q}$, $\boldsymbol{w_d}$ and $\boldsymbol{w_n}$ are treated as adjustable parameters. An increase in the ratio between $\boldsymbol{w_q}$ and $\boldsymbol{w_d}$ makes the filter slower in estimating the disturbance, while an increase in the ratio between $\boldsymbol{w_n}$ and $\boldsymbol{w_d}$ makes the estimator less sensitive to the output noise [35]. Even with this general insight of how to tune the variances, the proper selection of them is not trivial. In this work, the process covariance is modified to

$$W(\rho) = W_0 + \rho^2 B_{aug} B_{aug}^{\intercal}; \quad 0 \leq \rho \leq \infty, \tag{30}$$

as suggested by Doyle in [38]. The scalar parameter $\rho$ serves to handle effectively the trade-off between noise rejection and margin recovery. From preliminary simulations, the Kalman filter was tuned according to

$$var\{\boldsymbol{w_q}\} = \boldsymbol{0}_{n_q \times n_q} \tag{31}$$

$$var\{\boldsymbol{w_d}\} = 0.01^2 I_{n_d \times n_d} \tag{32}$$

$$var\{\boldsymbol{w_n}\} = (5 \times 10^{-6})^2 I_{n_y \times n_y} \tag{33}$$

$$\rho = 1 \tag{34}$$

$$L_{q,10\times5} \begin{cases} l_{q,1,1} = 0.39 \\ l_{q,2,2} = l_{q,3,3} = l_{q,4,4} = l_{q,5,5} = 0.54 \\ l_{q,2,4} = l_{q,3,5} = l_{q,4,2} = l_{q,5,3} = 0.12 \\ l_{q,6,1} = 24.69 \\ l_{q,7,2} = l_{q,8,3} = l_{q,9,4} = l_{q,10,5} = 479.20 \\ l_{q,7,4} = l_{q,8,5} = l_{q,9,2} = l_{q,10,3} = 179.24 \\ l_{q,i,j} = 0 \text{ elsewhere} \end{cases} \tag{35}$$

$$L_{d,5\times5} \begin{cases} l_{d,1,1} = 1638.95 \\ l_{d,2,2} = l_{d,2,4} = l_{d,3,3} = l_{d,3,5} = 1011.33 \\ l_{d,4,3} = l_{d,5,4} = -1144.51 \\ l_{d,4,5} = l_{d,5,2} = 1144.51 \\ l_{d,i,j} = 0 \text{ elsewhere.} \end{cases} \tag{36}$$

#### 4.3.1. Target selector

The augmented model lumps the plant-model mismatch into the external force estimates. If this mismatch persists over time and the desired reference is achieved ($\boldsymbol{y_{m_\infty}} = \boldsymbol{r}_\infty$) at steady state, a static relation is obtained from the estimator:

$$\underbrace{\begin{bmatrix} A - I & B \\ C & \boldsymbol{0}_{n_d \times n_u} \end{bmatrix}}_{A_t} \begin{bmatrix} \boldsymbol{q}_\infty \\ \boldsymbol{u}_\infty \end{bmatrix} = \begin{bmatrix} -B_d \hat{\boldsymbol{d}}_\infty \\ \boldsymbol{r}_\infty \end{bmatrix}. \tag{37}$$

This means that the state and inputs shall converge to $\boldsymbol{q}_\infty$ and $\boldsymbol{u}_\infty$ in steady state to compensate the plant-model mismatch. For this reason, $\boldsymbol{q}_\infty$ and $\boldsymbol{u}_\infty$ become state and input "target" in the OF-MPC formulation. Note that $(\boldsymbol{q}_\infty, \boldsymbol{u}_\infty)$ can be obtained from the knowledge of $\hat{\boldsymbol{d}}_\infty$ and $\boldsymbol{r}_\infty$. However, the estimator (Eq. 28) provides $\hat{\boldsymbol{d}}(t)$ at each time step $t$ but $\hat{\boldsymbol{d}}_\infty$ is needed to yield the targets. Assuming that the controller action is applied at time $t$, an anticipative action (preview) on the measured disturbance $\boldsymbol{d}(t)$, $\boldsymbol{d}(t+1)$, $\boldsymbol{d}(t+N+1)$ can be imposed by setting $\boldsymbol{d}(t+k) = \hat{\boldsymbol{d}}(t)$, $\forall\ k = 0, ..., N-1$ and hence $\hat{\boldsymbol{d}}_\infty \equiv \hat{\boldsymbol{d}}(t)$ (causal action, no preview). Thus, $\boldsymbol{q}_\infty$ and $\boldsymbol{u}_\infty$ can be obtained from Eq. 37. Note that $\boldsymbol{q}_\infty$ and $\boldsymbol{u}_\infty$ exist for any $\hat{\boldsymbol{d}}_\infty$ and $\boldsymbol{r}_\infty$ if the matrix $A_t$ has full rank.

### 4.4. OF-MPC formulation

Bleuler et al. proposed a procedure to set the control requirements in frequency domain based on a trade-off between the rotor response and the control effort [1]. With OF-MPC, the control requirements can be treated in a similar fashion, but in time-domain and using quadratic norms. OF-MPC offers a systematic way to optimally handle this compromise between control effort and controlled outputs by taking into account plant dynamics and constraints. The OF-MPC problem is formulated as

$$\begin{aligned} \min_u \quad & \frac{1}{2} (\boldsymbol{q}_N - \boldsymbol{q}_t)^{\intercal} P (\boldsymbol{q}_N - \boldsymbol{q}_t) \\ & + \frac{1}{2} \sum_{k=0}^{N-1} (\boldsymbol{q}_k - \boldsymbol{q}_t)^{\intercal} Q (\boldsymbol{q}_k - \boldsymbol{q}_t) \\ & + \frac{1}{2} \sum_{k=0}^{M-1} (\boldsymbol{u}_k - \boldsymbol{u}_t)^{\intercal} R (\boldsymbol{u}_k - \boldsymbol{u}_t) \end{aligned} \tag{38}$$

subj. to

$$\boldsymbol{q}_{k+1} = A\boldsymbol{q}_k + B\boldsymbol{u}_k + B_d\boldsymbol{d}_k, \quad k = 0, \ldots, N-1, \tag{39}$$

$$\boldsymbol{d}_{k+1} = \boldsymbol{d}_k, \quad k = 0, \ldots, N-1, \tag{40}$$

$$\boldsymbol{u}_k = \boldsymbol{u}_t, \quad k = M, \ldots, N-1, \tag{41}$$

$$K_u \boldsymbol{u}_k \leq \boldsymbol{i}_{max}, \quad k = 0, \ldots, M-1, \tag{42}$$

$$\boldsymbol{q}_0 = \hat{\boldsymbol{q}}(t), \tag{43}$$

$$\boldsymbol{d}_0 = \hat{\boldsymbol{d}}(t), \tag{44}$$

with targets $\boldsymbol{u}_t$, $\boldsymbol{q}_t$ given by

$$\begin{bmatrix} A - I & B \\ C & \boldsymbol{0}_{n_d \times n_u} \end{bmatrix} \begin{bmatrix} \boldsymbol{q}_t \\ \boldsymbol{u}_t \end{bmatrix} = \begin{bmatrix} -B_d \hat{\boldsymbol{d}}(t) \\ \boldsymbol{r}(t) \end{bmatrix}. \tag{45}$$

Matrices $Q \succeq 0$ and $R \succ 0$ are used to properly weight the trade-off between the rotor clearance and available bearing

capacity. They are selected in such a way that the rotor response consumes 25% of the available clearance $g_0$ and, at the same time, for the control effort to be 20% of the available bearing capacity (in terms of coil current):

$$Q = C' Q_y C;\ Q_y = diag(\boldsymbol{\alpha}) \frac{1}{(0.25 g_0)^2} I_{n_y \times n_y} \tag{46a}$$

$$R = (I_{n_u \times n_u} - diag(\boldsymbol{\alpha})) \frac{1}{(0.20 u_{max}^2)^2} I_{n_u \times n_u}, \tag{46b}$$

in which $n_u = 5$ and $n_y = 5$ are the number of inputs and measurements, respectively. The vector

$$\boldsymbol{\alpha} = [\alpha_z\ \alpha_{x_1}\ \alpha_{y_1}\ \alpha_{x_2}\ \alpha_{y_2}]$$

with

$$0 \leq \alpha_j \leq 1;\ j = z, x_1, y_1, x_2, y_2$$

is proposed to tune the aggressiveness of the controller around the nominal control requirement. Note that when $\alpha_j = 0.5$, the trade-off is that one expected from the "nominal" weights. For $\alpha_j \geq 0.5$, the controller becomes more aggressive along the $j$ direction. The control input weight $R$ involves the maximum control current $u_{j,max}$ which is set to 3.5 A to be consequent with the coil current limitation i.e., $u_{max} + i_0 = i_{max}$ in which $i_0 = 1.5$ A and $i_{max} = 5$ A. Hereinafter, $Q_0$ and $R_0$ denote the "nominal" weights on the states and inputs, respectively (i.e., when $\alpha_j = 0.5$).

The matrix $P$, calculated by means of the solution of the discrete algebraic Riccati equation

$$P = A^\intercal P A - (A^\intercal P B)(B^\intercal P B + R)^{-1}(B^\intercal P A) + Q, \tag{47}$$

establishes a terminal cost that guarantees nominal stability of the system. However, this term can deteriorate the optimality of the problem. Hence, it is not implemented in many practical applications, such as this case.

The prediction horizon $N = 30$ is selected to cover almost all the transient response. As seen in Eq. 38, a reduction of the control moves (i.e., control horizon $M \leq N$) is applied to limit the computation burden of the optimization problem, as suggested for embedded fast MPC applications. The input signal $\boldsymbol{u}$ is frozen and held constant after prediction time $M - 1$. A dedicated analysis of the controller execution time in a real microprocessor is done later to select the control moves.

Interestingly, the relation between *control currents* and *coil currents* is intrinsically considered in the problem formulation through the constraint in Eq. 42. In conical-shaped AMB systems, the current passing through each coil is a combination of "control efforts" in axial and radial directions. When using OF-MPC, the coils current limitations are known by the controller and hence optimally handled. However, if decentralized controllers were used, each controller would only limit their respective *control currents*, while the saturation of the real coil current would require a separate implementation. Thus, the problem is not addressed optimally.

### *4.5. OF-MPC controller as a QP problem*

Equations 39 to 41 allow eliminating the state sequence from the OF-MPC problem in Eqs. 38 to 44. Therefore, the optimal control problem can be expressed as the convex quadratic program (QP)

$$\min_{\mathbf{u}} \quad \frac{1}{2}\mathbf{u}^\intercal \mathcal{H} \mathbf{u} + [\mathcal{F}^\intercal(\boldsymbol{q} - \boldsymbol{q_t}) - \mathcal{H}^\intercal \mathbf{u}_t]^\intercal \mathbf{u} \tag{48}$$

subj. to

$$\mathcal{K}\mathbf{u} \leq \mathcal{I}, \tag{49}$$

in which $\mathbf{u} = [\boldsymbol{u}_0^*;\ ...;\ \boldsymbol{u}_{M-1}^*]$ is the optimization variable, $\mathbf{u}_t = [\boldsymbol{u_t}; ...; \boldsymbol{u_t}]$ stands for the input targets during the control horizon, $\mathcal{H} \in \mathbb{R}^{Mn_u \times Mn_u}$ is the Hessian matrix and $\mathcal{F} \in \mathbb{R}^{n_q \times Mn_u}$. The reader may refer to [39] or [40] for a detailed explanation of the QP problem formulation using a *batch approach*. The constraints in Eq. 49 are obtained by stating Eq. 42 for each time step from $k = 0$ to $k = M - 1$ as

$$\underbrace{\begin{bmatrix} K_u & 0 & 0 \\ 0 & \ddots & 0 \\ 0 & 0 & K_u \end{bmatrix}}_{\mathcal{K}} \mathbf{u} = \underbrace{\begin{bmatrix} \boldsymbol{i_{max}} \\ \vdots \\ \boldsymbol{i_{max}} \end{bmatrix}}_{\mathcal{I}}, \tag{50}$$

with $\mathcal{K} \in \mathbb{R}^{Mn_{coils} \times Mn_u}$ and $\mathcal{I} \in \mathbb{R}^{Mn_{coils} \times 1}$. Since the matrices defining the dynamics, costs, and constraints in Eqs. 48 and 49 do not vary during the execution of the OF-MPC controller (linear time-invariant (LTI) prediction model), the respective QP matrices can be precomputed offline. Every time step, the problem is updated with ($\boldsymbol{q}$, $\boldsymbol{q_t}$, $\boldsymbol{u_t}$) and then solved to get $\mathbf{u}$, but only the input $\boldsymbol{u}_0^*$ is applied to the plant due to the receding horizon principle of MPC.

As observed, applying OF-MPC requires solving the optimization problem in Eqs. 48 and 49 at every time step, based on the information of the estimated state and disturbances, and the state and input targets. A well-known technique for implementing fast MPC is to compute the entire control law offline, in which case the online controller can be implemented as a lookup table [41]. This method is named explicit MPC and works well for systems with small state and input dimensions (no more than five), few constraints, and short time horizons [42]. For larger systems such as the one studied in this paper, a variety of efficient algorithms already exists to solve the QP problem online. In this work, an online OF-MPC implementation is proposed using CVXGEN [43, 44], which is a C code Generator for embedded convex optimization and it is freely available for academia. In CVXGEN, the algorithm that solves the QP problem is based on a standard primal-dual interior-point method [44]. The CVXGEN code needed to formulate 48 - 49 is quite simple.

#### *4.5.1. Selecting the control moves*

To limit the computational burden in MPC, it is often useful to limit the control horizon by "blocking" control moves after a certain input horizon $M$, $1 \leq M < N$ [45].

Table 3: Execution time of the OF-MPC

| Control moves | NXP[1] (ms) | Infineon[2] (ms) | TI[3] (ms) |
|---|---|---|---|
| 2 | 0.095 | 0.62 | 1.83 |
| 3 | 0.213 | 1.56 | - |
| 4 | 0.392 | 2.78 | - |
| 5 | 0.645 | - | - |

[1] QorlQ P5020, 2 GHz (dSpace MicroLabBox)
[2] Infineon TC1793, 260 MHz (New Eagle GCM196)
[3] TMS320F28379D, 200 MHz (Texas Instruments LAUNCHXL-F28379D)

The larger the control moves $M$, the longer the computation time needed to solve the embedded QP problem. In fact, Eqs. 48 and 49 demonstrate how the QP problem dimension is strictly related to $M$.

In this research, a preliminary study was carried out to select the control moves. Benchmarks for three different processors were performed to verify the control implementation feasibility. Table 3 presents the execution time needed to solve the OF-MPC for $M = 2, ..., 5$.

Results in Tab. 3 indicate that the execution time is a quadratic function of the control moves. The plant under study is linearized with a sampling time $T_s = 0.25$ ms. Hence, the NXP QorlQ P5020 processor could be used for the OF-MPC with control moves up to $M = 3$ without the risk of overruns. However, due to the low-bandwidth mechanical dynamics of the system, larger time steps up to $T_s = 0.8$ ms are sufficient to control the plant. As such, off-the-shelf industrial processors such as the Infineon TC1793 become a feasible solution to implement OF-MPC. In contrast, the computational power of the TI TMS320F28379D processor is outperformed by the complexity of the control task, even with $M = 2$. In the following, we focus on the numerical and experimental validation of the OF-MPC strategy with $M = 2$, since it represents a worst-case scenario for the OF-MPC implementation.

## 5. Experimental results and discussion

Diverse experimental tests were conducted to validate the OF-MPC strategy through the test rig. Firstly, the lifting-up phase is presented to assess the controller during a very critical transient for the system. Secondly, output sensitivity tests were conducted to evaluate the control performance. Finally, the disturbance rejection properties of OF-MPC are compared with PIDs in the axial direction, i.e. the axis with the weakest force capability of the plant.

### 5.1. Test rig description

Figure 5 shows the plant under study together with other components needed for the experiments. A connection layout of the main components in the test bench is depicted in Fig. 6. Inside the control unit (dSpace MicroLabBox), a centralized position controller running at 4 kHz receives the air gap information from displacement sensors (Bently Nevada Proximitor 3300XL) and determines the corresponding current reference

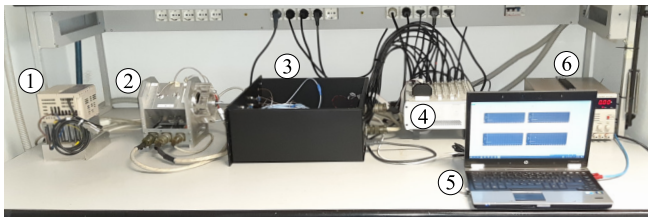


Figure 5: Test bench. (1) Motor driver, (2) Turbo-compressor on conical AMBs, (3) Power amplifier and sensor conditioning, (4) Control Unit: dSPACE MicroLabBox, (5) PC, (6) Power supply.

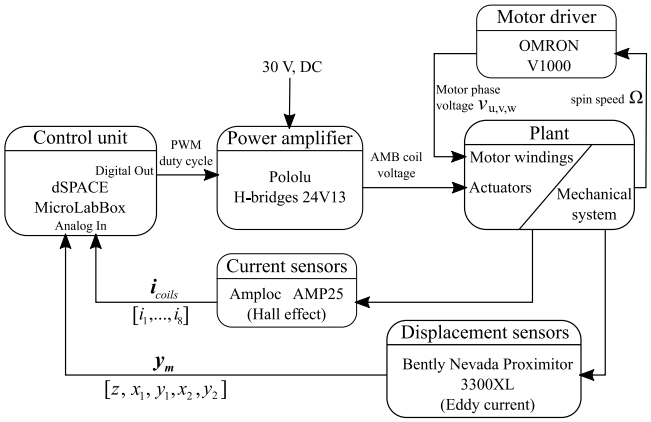


Figure 6: Block diagram of the test bench.

for each electromagnet. Inner PI current controllers take the current readings from Hall-effect probes (Amploc AMP25) and set the coil voltages by varying the PWM duty cycle on each power amplifier. Analog-to-digital conversion (16-bit resolution) of current and position signals is triggered by the PWM carrier waveform at 20 kHz. The power amplifier is constituted by eight Pololu 24V13 H bridges in locked-antiphase operation ($0 \div 100\%$ of duty cycle corresponds to $-30 \div 30$ V in the AMB coils). A two-pole induction motor is controlled with a variable-frequency driver (Omron V1000) to spin the compressor up to the maximum speed $\Omega_0 = 24$ krpm.

### 5.2. Lifting-up

The plant under study is a subsystem for an aircraft, which means that the rotor will lift up many times from any initial condition (in contact with back-up ball bearings) to the nominal air gap $g_0$ ($\boldsymbol{q} = \boldsymbol{0}$). Before the shaft lifts up, the coil current controllers are switched on and a bias current $i_0 = 1.5$ A is imposed on each coil. Subsequently, the position controller (OF-MPC + observer + target selector) is activated to steer the shaft to the nominal air gap.

Figure 7 depicts an experimental time history of the lifting-up phase with a transient response suitably damped. As observed from the zoomed area, the control inputs are such that the coil current saturation is optimally handled by the controller. The plant behavior during this phase is highly nonlinear, but a linear OF-MPC formulation combined with the full state observer resulted sufficient to steer the shaft properly. The target selector produces input targets based on the estimates to com-

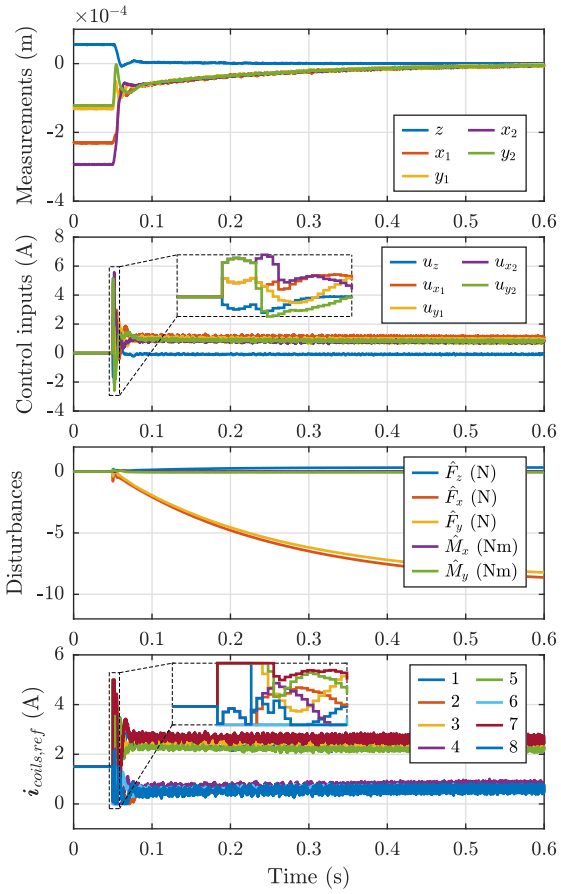


Figure 7: Transient response when the plant lifts-up. Control aggressiveness is set to $\alpha_j = 0.2$. The zoomed area evidences the coil current saturation together with the corresponding control inputs.

pensate the plant-model mismatch. In essence, this compensation produces an integral action and hence, zero-offset tracking is reached at steady state. The steady-state disturbances are not an accurate representation of the weight forces because estimates include a component due to the plant-model mismatch. Note that the disturbance estimate $\hat{\boldsymbol{d}}$ lumps uncertainties: force coefficients, actual air gaps on the plant and system geometry, among others. Nevertheless, the main contribution is attributed to the weight force compensation. Since the weight force is known from design, the deviations of the force estimate give an insight about the plant operation and the internal model of the controller.

### 5.3. Evaluation of the closed-loop performance

Output sensitivities were obtained experimentally by implementing a dual-channel Fast Fourier Transform analysis, as suggested in ISO 14839-3:2006 [32]. A swept sine noise

$$\boldsymbol{w_n} = [w_{n_z},\ w_{n_{x_1}},\ w_{n_{y_1}},\ w_{n_{x_2}},\ w_{n_{y_2}}]^\intercal$$

was injected on each measurement channel (one by one) and then both the injected noise and the corrupted output measurement were recorded. This process is repeated for each channel $(z,\ x_1,\ y_1,\ x_2,\ y_2)$ to obtain the corresponding output sensitivity functions

$$\begin{aligned} S_z(f) &= \frac{z(f)}{w_{n_z}(f)}, \\ S_{x_1}(f) &= \frac{x_1(f)}{w_{n_{x_1}}(f)},\ S_{y_1}(f) = \frac{y_1(f)}{w_{n_{y_1}}(f)}, \\ S_{x_2}(f) &= \frac{x_2(f)}{w_{n_{x_2}}(f)},\ S_{y_2}(f) = \frac{y_2(f)}{w_{n_{y_2}}(f)}. \end{aligned} \tag{51}$$

which are used as the indicator of closed-loop performance.

The functions $\mathcal{S} = \{S_z,\ S_{x_1},\ S_{y_1},\ S_{x_2},\ S_{y_2}\}$ were experimentally obtained for different control requirements (i.e., varying $\alpha_j$) and using the observer presented in Eqs. 31 to 36. Figure 8 shows how the aggressiveness of the controller changes for $\alpha_j = \{0.2,\ 0.5,\ 0.8\}$. The low-frequency disturbance rejection deteriorates considerably when $\alpha_j = 0.2$. It improves with $\alpha_j = 0.5$ and $\alpha_j = 0.8$ but better noise attenuation is achieved with $\alpha_j = 0.5$. In general, the best trade-off between disturbance rejection and noise attenuation is observed with $\alpha_j = 0.5$. Nevertheless, all peak values of the sensitivity functions are below 9.5 dB and hence considered acceptable for unrestricted long-term operation [32].

### 5.4. Comparison of OF-MPC with PIDs

Decentralized PID controllers were obtained by eliminating the inequality constraints from the OF-MPC formulation. The idea is to generate PID controllers for each DOF that behave as close as possible to the OF-MPC in the vicinity of the steady state condition [40]. A similar method was proposed by Lee in [21] to generate decoupled control action using an LQR design approach.

Firstly, the inequality constraint in problem 48 - 49 is eliminated. Since $R \succ 0$, $\mathcal{H} \succ 0$, Eq. 48 is a positive definite quadratic function of $\mathbf{u}$. Therefore, its minimum can be found by computing its gradient and equating it to zero

$$\mathbf{u} = -\mathcal{H}^{-1}\mathcal{F}^\intercal(\boldsymbol{q}(0) - \boldsymbol{q}_t) + \mathbf{u}_t \tag{52}$$

where $\mathbf{u}(t) = \left\{\boldsymbol{u}_0^*, \ldots, \boldsymbol{u}_{M-1}^*\right\}$. Since only the first control in this sequence ($\boldsymbol{u}(t) = \boldsymbol{u}_0^*$) is applied to the plant, then

$$\boldsymbol{u}_{0,uc}^* = -K(\boldsymbol{q}(0) - \boldsymbol{q}_t) + \boldsymbol{u}_t, \tag{53}$$

where $K^{n_u \times n_q}$ is defined as the first $n_u$ rows of the matrices $\mathcal{H}^{-1}\mathcal{F}^\intercal$. The control action from Eq. 53 can be interpreted as a coupled unconstrained discrete-time optimal controller obtained over a finite horizon. If the resulting $K$ is such that the matrix $(A - BK)$ is Hurwitz, i.e. all its eigenvalues have moduli smaller than one [40], the plant is closed-loop stable. The terms $\boldsymbol{u}_t$ denote a small integral action added from the knowledge of the plant-model mismatch.

Note that the state vector $\boldsymbol{q}$ is constituted by the five controlled displacements and their derivatives:

$$\boldsymbol{q} = [z,\ x_1,\ y_1,\ x_2,\ y_2\ \dot{z},\ \dot{x}_1,\ \dot{y}_1,\ \dot{x}_2,\ \dot{y}_2]^\intercal.$$

Hence the term $(\boldsymbol{q}(0) - \boldsymbol{q}_t)$ represents the displacement errors and the error derivatives (by definition, $\boldsymbol{q}_t$ stands for the steady

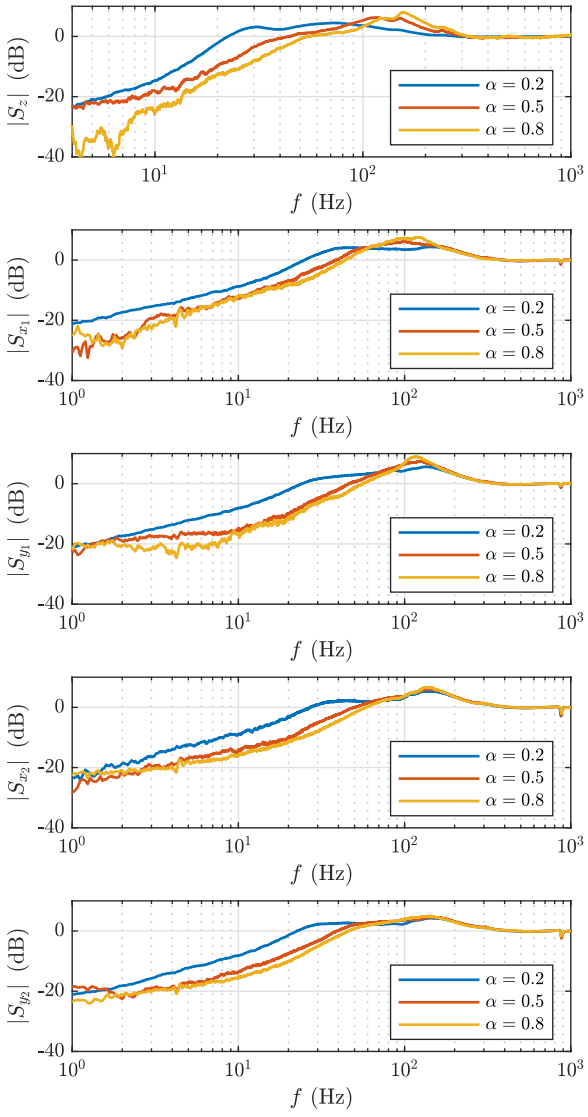


Figure 8: Output sensitivities on $z$, $x_1$, $y_1$, $x_2$ and $y_2$ for different grades of controller aggressiveness $\alpha_{z,x_1,y_1,x_2,y_2} \equiv \alpha$. Each test is performed independently on each measurement channel by injecting a sweep noise with a frequency that varies from 0.1 Hz to 1 kHz and amplitude 10 $\mu$m.

state references). Therefore, decentralized PD controller gains can be extracted from $K$. By setting the control aggressiveness to $\alpha_{z,x_1,y_1,x_2,y_2} = 0.2$, for instance, and recalculating the corresponding matrices $\mathcal{H}$, $\mathcal{F}$ of the QP problem, the state feedback gain results:

$$K_{5\times10}\begin{cases} k_{1,1} = 9911 \\ k_{1,6} = 49 \\ k_{2,2} = k_{3,3} = k_{4,4} = k_{5,5} = 21390 \\ k_{2,4} = k_{3,5} = k_{4,2} = k_{5,3} = 3576 \\ k_{2,7} = k_{3,8} = k_{4,9} = k_{5,10} = 79 \\ k_{2,9} = k_{3,10} = k_{4,7} = k_{5,8} = 9 \\ k_{i,j} = 0 \text{ elsewhere.} \end{cases} \tag{54}$$

Table 4 shows the proportional and derivative gains extracted from matrix $K$. A cut-off derivative filter, with a time constant $\tau_f$ ten times lower than the derivative one, was added to each PD controller. Figure 9 shows the control layout of both decentralized and OF-MPC controllers. A small integral action $\boldsymbol{u}_t$ is added to the PD actions to guarantee zero-offset tracking from the knowledge of the plant-model mismatch. The decentralized control results in PID controllers, one for each degree of freedom of the plant. The target selector, which serves to generate the integral action, is that presented in Eq. 37.

Table 4: Decentralized PD controllers ($\alpha_{z,x_1,y_1,x_2,y_2} = 0.2$)

| Controller | $K_p$ (A/m) | $K_d$ (A/m/s$^2$) | $1/\tau_f$ (s$^{-1}$) |
|---|---|---|---|
| PD$_z$ | 9911 | 49 | 2000 |
| PD$_{z,x_1,y_1,x_2,y_2}$ | 21390 | 79 | 2700 |

Regarding the OF-MPC implementation (see control layout in Fig. 9), the plant states were defined as the measurements $[z,\ x_1,\ y_1,\ x_2,\ y_2]$, together with their rate of variation $[\dot{z},\ \dot{x}_1,\ \dot{y}_1,\ \dot{x}_2,\ \dot{y}_2]$. The calculation of the derivatives is filtered at the same cut-off frequency presented in Tab. 4. Hence only a reduced version of the observer presented in Eqs. 31 to 36 is used to get $\hat{\boldsymbol{d}}$. The choice of a reduced observer serves to perform a fair comparison between OF-MPC and PIDs because in this case the Kalman filter dynamics will not affect the control loop shape.

A comparison of the control performance when using full state estimation and a reduced version is not the scope of this work. However, according to [46], poor pass-band robustness in a full-order state estimator can be improved, to some extent, by using a reduced-order observer with direct feedthrough of plant outputs.

An experimental comparison of the output sensitivities when using PID and OF-MPC controllers is presented in Fig. 10 for ($\alpha_{z,x_1,y_1,x_2,y_2} = 0.2$). Each test is performed independently on each measurement channel by injecting a swept sine noise with a frequency that varies from 0.1 Hz to 1 kHz and amplitude 10 $\mu$m. Both controllers present similar frequency responses nearby the nominal operating point, which suggests that decentralized controllers could still be designed from the OF-MPC formulation when computational overhead is a bottleneck.

### *5.4.1. Impact test in the axial direction*

One of the main drawbacks of cone-shaped AMB systems is their low axial force generation capability. Notable differences in the transient response are obtained when using PIDs or OF-MPC controllers and the coil current limits are reached. Figure 11 shows preliminary simulation results of impact tests in the axial direction. Both the controllers are designed with $\alpha_{x_1,y_1,x_2,y_2} = 0.2$ and $\alpha_z = 0.4$ and the plant was simulated using the nonlinear system in Eq. 12. A saturation stage limits the coil currents when PID controllers are used (i.e., $0 \leq i_{coils} \leq 5$ A). The upper saturation is not necessary in the OF-MPC case because the current limits are already known by the controller (see problem formulation in Eq. 42).

The system behaves similarly with OF-MPC (Fig. 11a) and PID (Fig. 11b) controllers when low impacts are applied. Conversely, in Figs. 11c and 11d, the coil currents saturate when

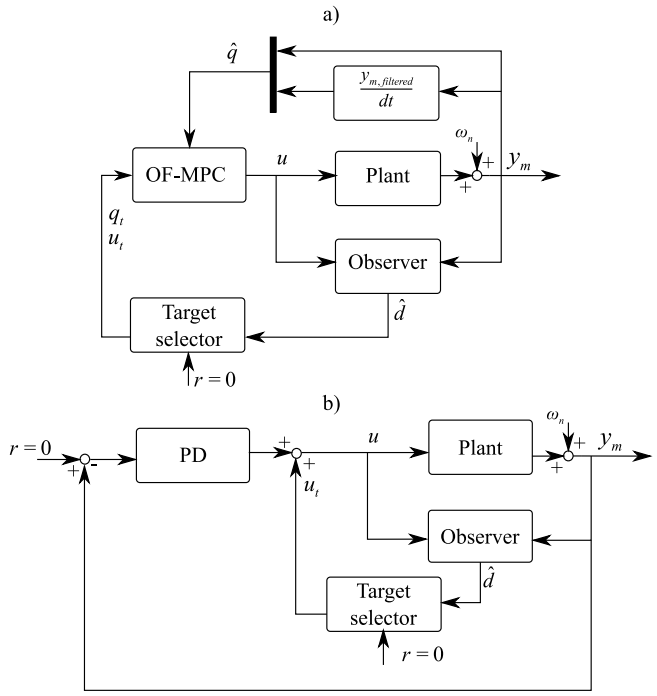


Figure 9: a) OF-MPC with a reduced observer (RO) i.e., only the disturbance estimates $\hat{\boldsymbol{d}}$ are obtained from the observer, $\hat{\boldsymbol{q}}$ is obtained directly from the measurements. b) Control scheme with PID controllers. The integral action is identical to that of the OF-MPC.

a more intense impact is applied and larger air gap values are attained in both cases.

In fact, for a similar axial deviation, the radial displacement of the rotor does not exceed 0.1 mm when using OF-MPC (see Fig. 11c) while it becomes three times larger when using PIDs (see Fig. 11d). Note also that OF-MPC handles more effectively the coil current upper saturation which lasts longer with PID.

To compare experimentally the OF-MPC and the PIDs when the system reacts to an axial disturbance force, the axial control action is modified to

$$u_{z,disturbed} = u_z + u_{d,z},$$

where $u_{d,z}$ is a disturbance current used to perturb the plant in axial direction. Figures 12 to 14 show transient responses for two levels of disturbance forces and different aggressiveness values for the controllers.

Low controller aggressiveness values in all the directions ($\alpha_{z,x_1,y_1,x_2,y_2} = 0.2$) yield similar transient behavior for a current disturbance $u_{d,z,max} = 4$ A in both OF-MPC and PID cases (Figs. 12a and 12b). However, Figs. 12c and 12d show that, with a larger axial disturbance $u_{d,z,max} = 5$ A, the OF-MPC system produces a more contained overshoot (56%) when compared to the PID variant.

As expected, with a more aggressive control action in the axial direction (i.e., $\alpha_z = 0.4$), the axial deviations in Figs. 13a and 13b halved those in the previous test (Fig. 12a and 12b). However, the radial deviations were severely affected, with the PID variant being noticeably worse than OF-MPC. A comparison between Figs. 13a and 13b shows that the maximum deviations when using PIDs resulted 50 % and 20 % larger than OF-MPC ones in $(x_1, y_1)$ and $(x_2, y_2)$, respectively. Also, the upper coil current saturation lasts for a longer time interval when using PIDs. Thus, OF-MPC offers a more favorable saturation handling by intrinsically taking it into account and considering the trade-off between control efforts and air gap deviation. When a large-amplitude disturbance signal is applied, the PID-controlled plant response presented in Fig. 13d reached a critical condition because the shaft almost reached a mechanical impact condition with the back-up ball bearings (radial deflection of 0.22 mm). A more favorable behavior was obtained with the OF-MPC, where the overall displacement of the rotor did not exceed 0.15 mm.

By comparing Figs. 12 and 14, it is also evident that OF-

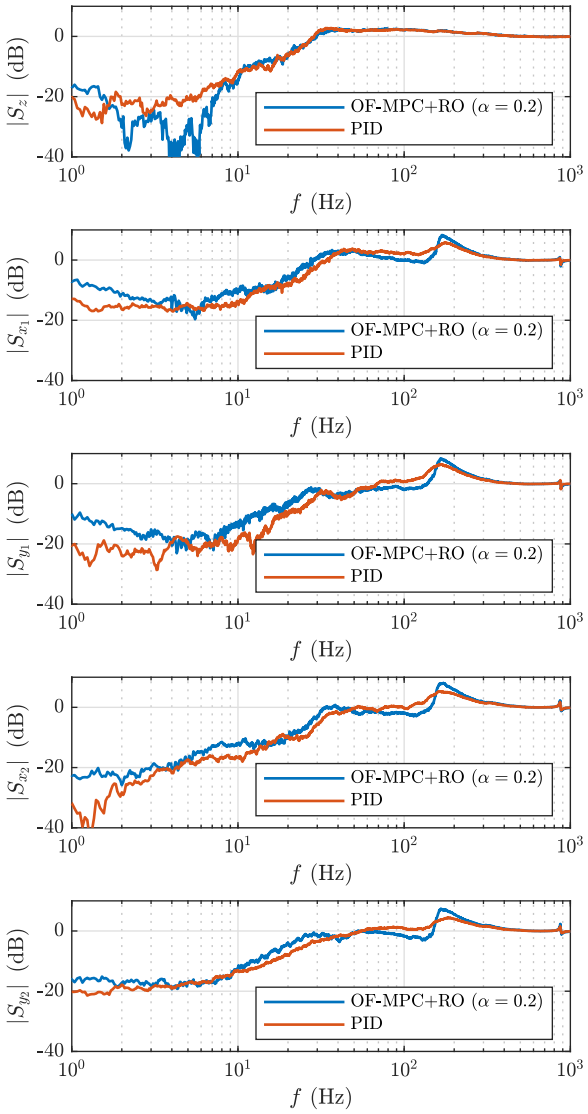


Figure 10: Output sensitivities on $z$, $x_1$, $y_1$, $x_2$ and $y_2$ from a comparison of the OF-MPC + reduced observer (RO) with decentralized PID controllers. Each test is performed independently on each measurement channel by injecting a swept sine noise with a frequency that varies from 0.1 Hz to 1 kHz and an amplitude 10 $\mu$m.

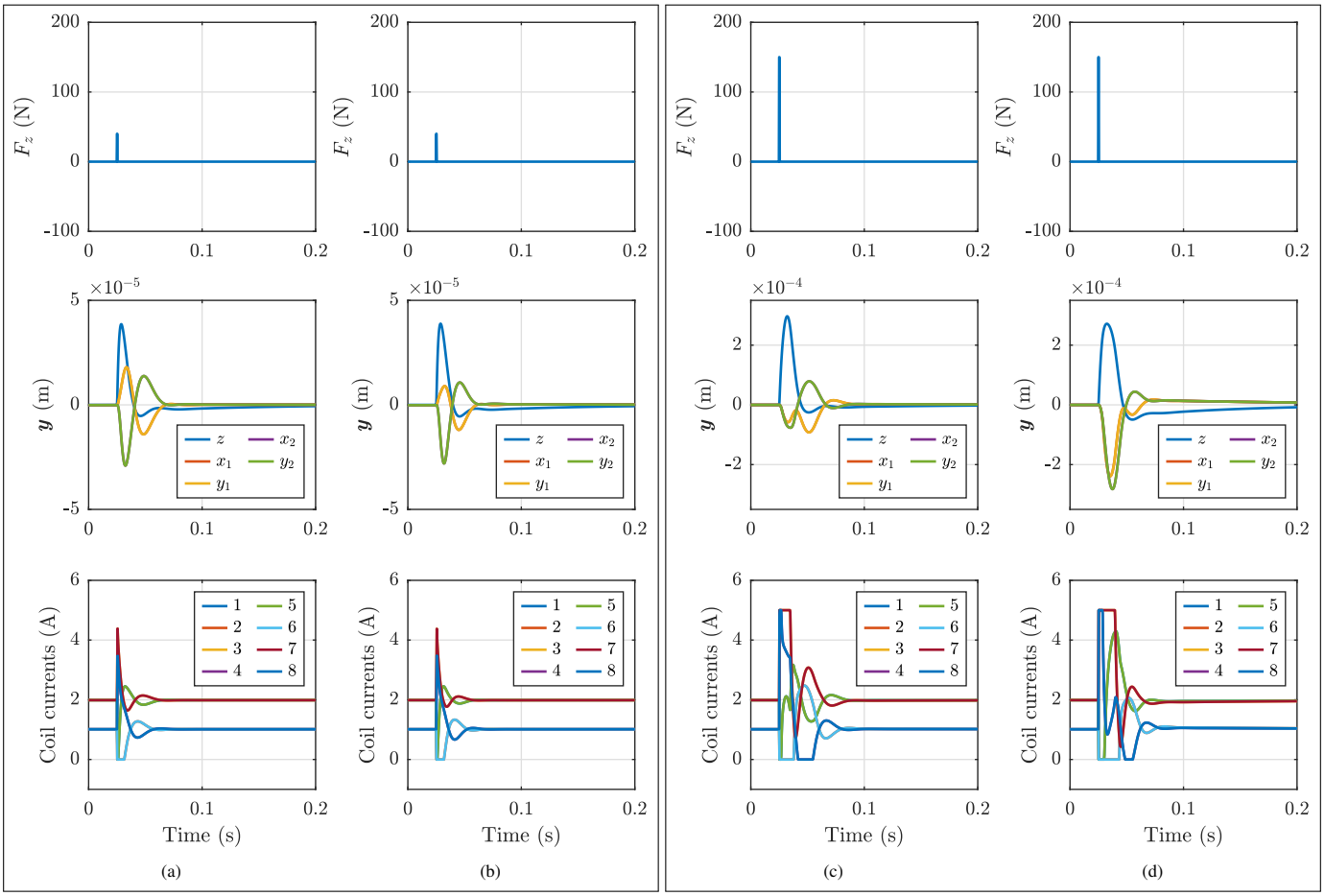


Figure 11: Simulation of an impact in axial direction. A low impact is applied in a) with an OF-MPC controller and b) with PIDs. The responses to larger impacts are presented in c) for OF-MPC and in d) for PIDs. Both the controllers are designed with $\alpha_{x_1,y_1,x_2,y_2} = 0.2$ and $\alpha_z = 0.4$. The rotor deviates much more when PIDs are used and the upper coil current limitations are reached.

MPC outperforms PIDs when the aggressiveness in radial direction is increased from $\alpha_{x_1,y_1,x_2,y_2} = 0.2$ to $\alpha_{x_1,y_1,x_2,y_2} = 0.3$. With OF-MPC (Fig. 14a), the maximum radial deviations were attenuated to 70% of those with PIDs (Fig. 14b). For a larger disturbance, the radial air gap deviations with PIDs in Fig. 14d almost doubled those with OF-MPC in Fig. 14c.

For both OF-MPC and PID control techniques, the implementation of more aggressive control actions was not experimentally feasible because the measurement noise is fed back into the control loop by the compensators. This effect is evident when inspecting the coil current reference waveforms, as the noise tends to be directly proportional to the control aggressiveness $\alpha_j$. In the particular case of the OF-MPC, this issue can be addressed with a full-state estimation, as presented in Secs. 5.2 and 5.3. In such case, the trade-off between noise rejection and margin recovery can be handled effectively by tuning through repeated experiments the parameter $\rho$ from Eq. 30.

### *5.5. Rotordynamics*

The effectiveness of the controller during rotation was validated by running the plant up to the maximum spin speed $\Omega_0 = 24$ krpm. Note that the OF-MPC is based on a linearized plant model obtained at standstill ($\Omega = 0$) as detailed in Sec. 4.1. This means that the variation of the plant due to gyroscopic effects is not known to the controller. Nevertheless, the OF-MPC performed properly within the speed range of interest.

On the other hand, the unbalance forces resulted very small due to proper machining quality and balancing of the rotor, and hence no additional control action was advised during operation at different speeds.

Finally, we point out that the augmented state estimator used by the OF-MPC is not dedicated to estimate unbalance forces. The rotor unbalance causes force disturbances that vary harmonically with the rotational speed of the machine, whereas OF-MPC estimates low-frequency load variations, i.e. persistent additive disturbances to lump all into a plant-model mismatch estimate. During the OF-MPC control design phase, it is assumed that the rotor has a proper balancing quality grade as suggested by the ISO 1940 standard [47].

## 6. Conclusions

The present paper dealt with the design, implementation and experimental validation of an offset-free model predictive control (OF-MPC) for conical active magnetic bearings (AMB). A sound theoretical framework was established to support the

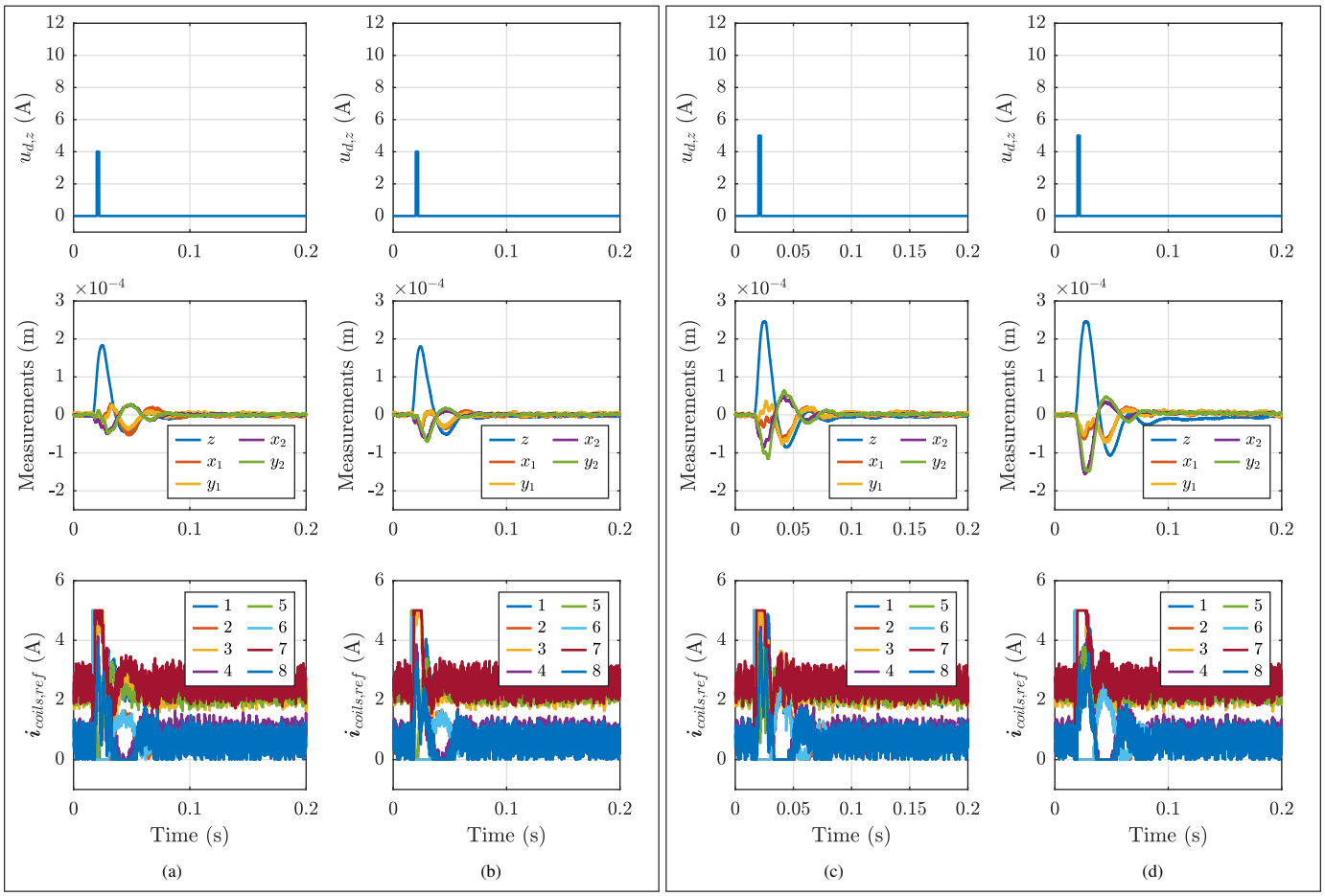


Figure 12: OF-MPC and PID comparison when an short-time impact force is applied in axial direction when using a) OF-MPC and b) PIDs. A response to a higher disturbance is present in c) for an OF-MPC and in d) for PIDs. Both OF-MPC and PIDs controllers are tuned with $\alpha_{z,x_1,y_1,x_2,y_2} = 0.2$.

synthesis of the control strategy. Subsequently, the control was implemented and tested in a downscaled version of a turbo-compressor for aircraft use.

From an experimental perspective, the OF-MPC strategy was compared with decentralized PIDs. A fair benchmark was performed by synthesizing the PIDs from the OF-MPC problem formulation. It was shown that, due to its centralized nature, the OF-MPC is particularly suitable to optimally handle the plant-model mismatch together with coil current limitations. Furthermore, results demonstrate the potential of OF-MPC for cone-shaped AMB systems, since the coupling of radial and axial control actions and the low force generation capability in the axial direction are aspects intrinsically handled by the controller. OF-MPC resulted a promising constrained optimal control technique that outperformed decentralized PID controllers in terms of axial disturbance rejection. This feature gives a fundamental advantage in cone-shaped AMBs, where the axial force capability is low and thus particularly sensitive to disturbances.

## References


[1] H. Bleuler, M. Cole, P. Keogh, R. Larsonneur, E. Maslen, Y. Okada, G. Schweitzer, A. Traxler, et al., Magnetic bearings: theory, design, and application to rotating machinery, Springer Science & Business Media, 2009.

[2] A. Chiba, T. Fukao, O. Ichikawa, M. Oshima, M. Takemoto, D. G. Dorrell, Magnetic bearings and bearingless drives, Elsevier, 2005.

[3] A. Filatov, L. Hawkins, P. McMullen, Homopolar permanent-magnet-biased actuators and their application in rotational active magnetic bearing systems, in: Actuators, Vol. 5, Multidisciplinary Digital Publishing Institute, 2016, p. 26.

[4] S.-L. Chen, C.-C. Weng, Robust control of a voltage-controlled three-pole active magnetic bearing system, IEEE/ASME Transactions on Mechatronics 15 (3) (2010) 381–388.

[5] S. Circosta, R. Galluzzi, A. Bonfitto, L. Castellanos, N. Amati, A. Tonoli, Modeling and validation of the radial force capability of bearingless hysteresis drives, in: Actuators, Vol. 7, Multidisciplinary Digital Publishing Institute, 2018, p. 69.

[6] M. D. Noh, E. H. Maslen, Self-sensing magnetic bearings using parameter estimation, IEEE Transactions on Instrumentation and Measurement 46 (1) (1997) 45–50.

[7] M. Noh, W. Gruber, D. L. Trumper, Low-cost eddy-current position sensing for bearingless motor suspension control, in: Electric Machines and Drives Conference (IEMDC), 2017 IEEE International, IEEE, 2017, pp. 1–6.

[8] A. Bonfitto, A. Tonoli, M. Silvagni, Sensorless active magnetic dampers for the control of rotors, Mechatronics 47 (2017) 195–207.

[9] C. Lusty, P. Keogh, Active vibration control of a flexible rotor by flexibly mounted internal-stator magnetic actuators, IEEE/ASME Transactions on Mechatronics 23 (6) (2018) 2870–2880.

[10] S. Lei, A. Palazzolo, Control of flexible rotor systems with active magnetic bearings, Journal of Sound and Vibration 314 (1-2) (2008) 19–38.

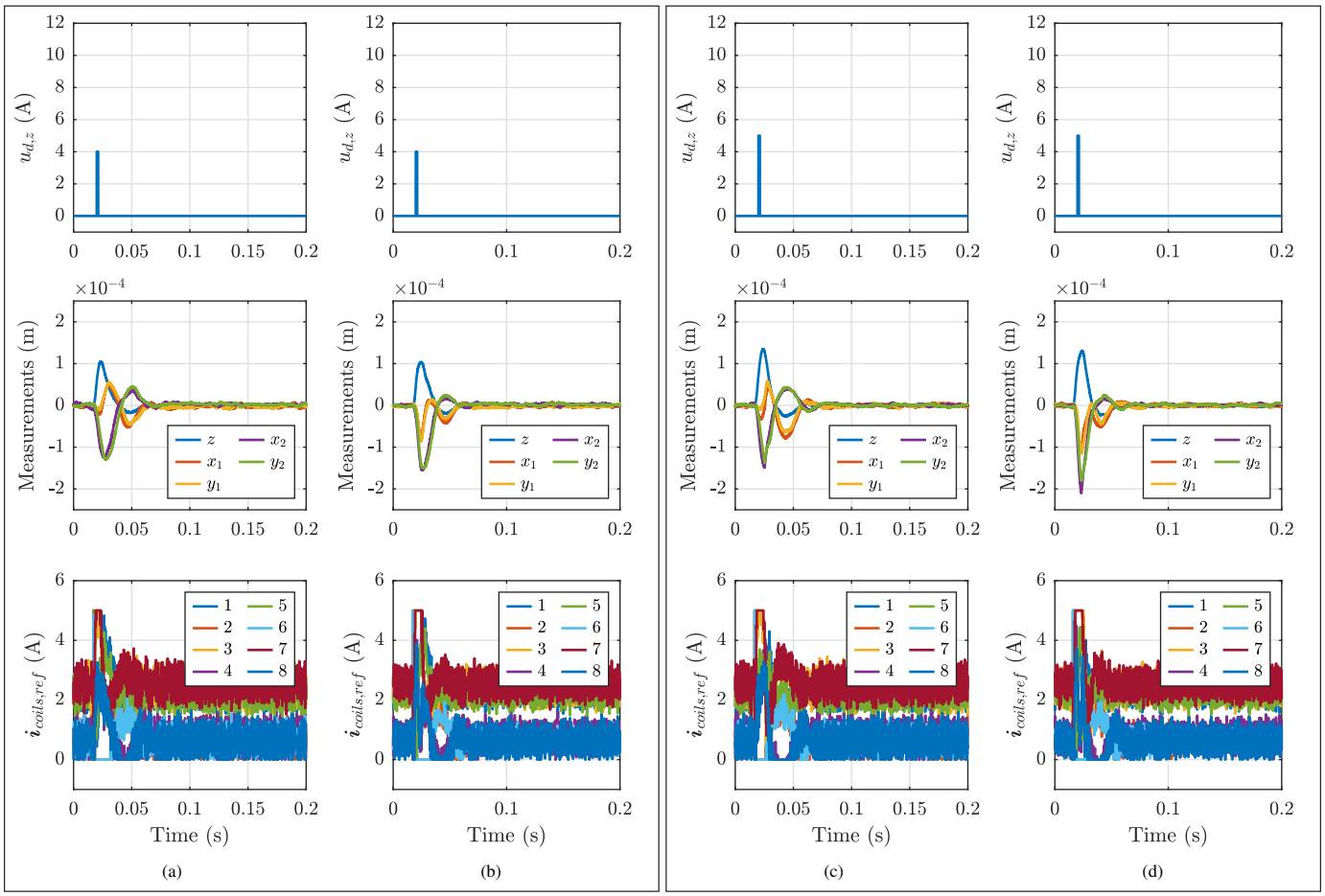


Figure 13: OF-MPC and PID comparison when an short-time impact force is applied in axial direction when using a) OF-MPC and b) PIDs. A response to a higher disturbance is present in c) for an OF-MPC and in d) for PIDs. Both OF-MPC and PIDs controllers are tuned with $\alpha_z = 0.4$, $\alpha_{x_1,y_1,x_2,y_2} = 0.2$.


[11] A. Bonfitto, L. Castellanos Molina, A. Tonoli, N. Amati, Offset-free model predictive control for active magnetic bearing systems, in: Actuators, Vol. 7, Multidisciplinary Digital Publishing Institute, 2018, p. 46.

[12] W. Gruber, R. Remplbauer, E. Göbl, Design of a novel bearingless permanent magnet vernier slice motor with external rotor, in: 2017 IEEE International Electric Machines and Drives Conference (IEMDC), IEEE, 2017, pp. 1–6.

[13] M. Noh, W. Gruber, D. L. Trumper, Hysteresis bearingless slice motors with homopolar flux-biasing, IEEE/ASME Transactions on mechatronics 22 (5) (2017) 2308–2318.

[14] S. Circosta, A. Bonfitto, C. Lusty, P. Keogh, N. Amati, A. Tonoli, Analysis of a shaftless semi-hard magnetic material flywheel on radial hysteresis self-bearing drives, in: Actuators, Vol. 7, Multidisciplinary Digital Publishing Institute, 2018, p. 87.

[15] Y. Ishino, T. Mizuno, M. Takasaki, M. Hara, D. Yamaguchi, Development of a compact axial active magnetic bearing with a function of two-tilt-motion control, in: Actuators, Vol. 6, Multidisciplinary Digital Publishing Institute, 2017, p. 14.

[16] A. Bonfitto, G. Botto, M. Chiaberge, L. Suarez, A. Tonoli, A multipurpose control and power electronic architecture for active magnetic actuators, in: 2012 15th International Power Electronics and Motion Control Conference (EPE/PEMC), IEEE, 2012, pp. DS2b–9.

[17] S. Xu, J. Fang, A novel conical active magnetic bearing with claw structure, IEEE Transactions on Magnetics 50 (5) (2013) 1–8.

[18] A. Katyayn, P. K. Agarwal, Comparative analysis of conical and conventional active magnetic bearings for complete support of a 5-dof rotor system, in: 2017 International Conference on Advances in Mechanical, Industrial, Automation and Management Systems (AMIAMS), IEEE, 2017, pp. 53–58.

[19] W. Zhang, H. Zhu, Radial magnetic bearings: An overview, Results in physics 7 (2017) 3756–3766.

[20] Y. Jing, Y. Lie, X. Jing, Coupled dynamics and control of a rotor-conical magnetic bearing system, Proceedings of the Institution of Mechanical Engineers, Part J: Journal of Engineering Tribology 220 (7) (2006) 581–586.

[21] C.-W. Lee, H.-S. Jeong, Dynamic modeling and optimal control of cone-shaped active magnetic bearing systems, Control Engineering Practice 4 (10) (1996) 1393–1403.

[22] L.-C. Lin, T.-B. Gau, Feedback linearization and fuzzy control for conical magnetic bearings, IEEE Transactions on Control Systems Technology 5 (4) (1997) 417–426.

[23] S.-J. Huang, L.-C. Lin, Fuzzy modeling and control for conical magnetic bearings using linear matrix inequality, Journal of Intelligent and Robotic systems 37 (2) (2003) 209–232.

[24] J. B. Rawlings, D. Q. Mayne, M. Diehl, Model Predictive Control: Theory, Computation, and Design, Nob Hill Publishing, 2017.

[25] T. Bächle, S. Hentzelt, K. Graichen, Nonlinear model predictive control of a magnetic levitation system, Control Engineering Practice 21 (9) (2013) 1250 – 1258.

[26] M. Klaučo, M. Kalúz, M. Kvasnica, Real-time implementation of an explicit mpc-based reference governor for control of a magnetic levitation system, Control Engineering Practice 60 (2017) 99–105.

[27] C. Zhang, K. Tseng, Y. Xiao, K. Zhu, Model-based predictive control for a compact and efficient flywheel energy storage system with magnetically assisted bearings, in: 2004 IEEE 35th Annual Power Electronics Specialists Conference (IEEE Cat. No. 04CH37551), Vol. 5, IEEE, 2004, pp. 3573–3579.

[28] Y.-W. Tsai, P. Van Duc, V. A. Duong, N. C. Trang, T. D. Chu, Model

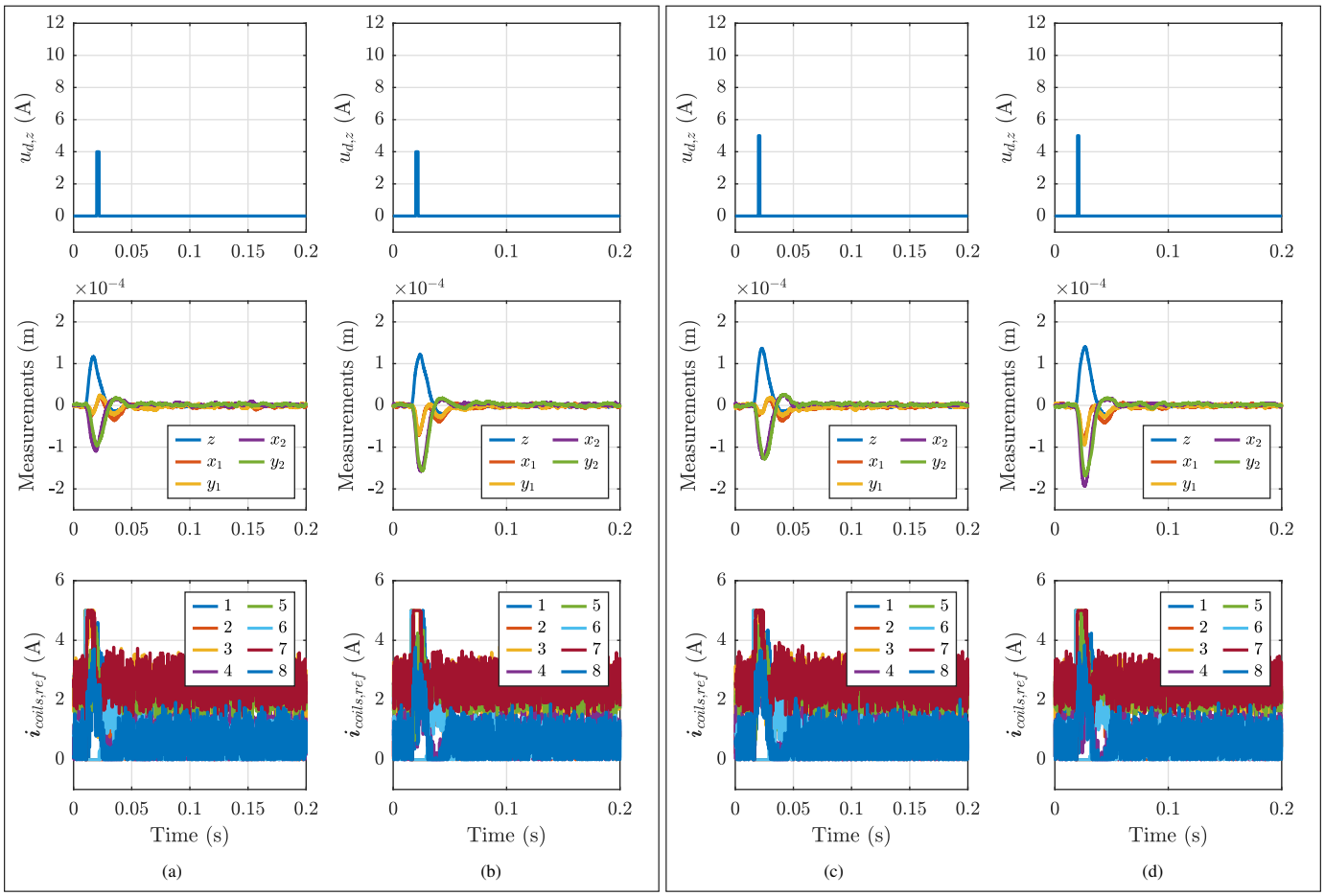


Figure 14: OF-MPC and PID comparison when an short-time impact force is applied in axial direction when using a) OF-MPC and b) PIDs. A response to a higher disturbance is present in c) for an OF-MPC and in d) for PIDs. Both OF-MPC and PIDs controllers are tuned with $\alpha_z = 0.4$, $\alpha_{x_1,y_1,x_2,y_2} = 0.3$.

predictive control nonlinear system of active magnetic bearings for a flywheel energy storage system, in: AETA 2015: Recent Advances in Electrical Engineering and Related Sciences, Springer, 2016, pp. 541–551.

[29] U. Maeder, F. Borrelli, M. Morari, Linear offset-free model predictive control, Automatica 45 (10) (2009) 2214–2222.

[30] G. Pannocchia, Offset-free tracking mpc: A tutorial review and comparison of different formulations, in: 2015 European Control Conference (ECC), IEEE, 2015, pp. 527–532.

[31] F. Borrelli, M. Morari, Offset free model predictive control, in: 2007 46th IEEE Conference on Decision and Control, IEEE, 2007, pp. 1245–1250.

[32] ISO 14839-3:2006. Mechanical vibration – Vibration of rotating machinery equipped with active magnetic bearings – Part 3: Evaluation of stability margin.

[33] G. Genta, Vibration of structures and machines: practical aspects, Springer Science & Business Media, 2012.

[34] G. Pannocchia, J. B. Rawlings, Disturbance models for offset-free model-predictive control, AIChE Journal 49 (2) (2003) 426–437.

[35] G. Pannocchia, N. Laachi, J. B. Rawlings, A candidate to replace pid control: Siso-constrained lq control, AIChE Journal 51 (4) (2005) 1178–1189.

[36] K. R. Muske, T. A. Badgwell, Disturbance modeling for offset-free linear model predictive control, Journal of Process Control 12 (5) (2002) 617–632.

[37] G. Pannocchia, E. C. Kerrigan, Offset-free control of constrained linear discrete-time systems subject to persistent unmeasured disturbances, in: 42nd IEEE International Conference on Decision and Control (IEEE Cat. No. 03CH37475), Vol. 4, IEEE, 2003, pp. 3911–3916.

[38] J. Doyle, G. Stein, Robustness with observers, IEEE transactions on automatic control 24 (4) (1979) 607–611.

[39] F. Borrelli, A. Bemporad, M. Morari, Predictive Control for Linear and Hybrid Systems, Cambridge University Press, 2017.

[40] G. Goodwin, M. M. Seron, J. A. De Doná, Constrained control and estimation: an optimisation approach, Springer Science & Business Media, 2006.

[41] A. Alessio, A. Bemporad, A survey on explicit model predictive control, in: Nonlinear model predictive control, Springer, 2009, pp. 345–369.

[42] Y. Wang, S. Boyd, Fast model predictive control using online optimization, IEEE Transactions on control systems technology 18 (2) (2009) 267–278.

[43] J. Mattingley, Y. Wang, S. Boyd, Code generation for receding horizon control, in: 2010 IEEE International Symposium on Computer-Aided Control System Design, IEEE, 2010, pp. 985–992.

[44] J. Mattingley, S. Boyd, Cvxgen: A code generator for embedded convex optimization, Optimization and Engineering 13 (1) (2012) 1–27.

[45] A. Bemporad, P. Patrinos, Simple and certifiable quadratic programming algorithms for embedded linear model predictive control, IFAC Proceedings Volumes 45 (17) (2012) 14–20.

[46] B. D. Anderson, J. B. Moore, Optimal control: linear quadratic methods, Courier Corporation, 2007.

[47] ISO 1940:1986. Mechanical Vibration – Balancing Quality Requirements of Rigid Rotors.